# C–C and C–H coupling reactions by Fe$_3$O$_4$/KCC-1/ APTPOSS supported palladium-salen-bridged ionic networks as a reusable catalyst

Asadollah Hassankhani,[*a] Seyed Mohsen Sadeghzadeh [ID][b] and Rahele Zhiani[b]

This study investigates the potential application of an efficient, easily recoverable and reusable magnetically separable Fe$_3$O$_4$/KCC-1/APTPOSS nanoparticle-supported salen/Pd(II) catalyst for C–C and C–H cross-couplings. The Fe$_3$O$_4$/KCC-1/APTPOSS/salen/Pd(II) MNPs were thoroughly characterized by using TEM, FE-SEM, TGA, XRD, VSM, FT-IR, ICP-MS, and BET. This observation was exploited in the direct and selective chemical reaction of 2-acetyl-benzaldehyde with cyclopentadiene for the synthesis of pentafulvene. The recycled catalyst has been analyzed by ICP-MS showing only minor changes in the morphology after the reaction, thus confirming the robustness of the catalyst.

## Introduction

Schiff bases are a significant class of ligands and have been studied heavily. Much effort has been made to investigate the sustainability of Schiff-base type ligands for coupling reactions. The half-salen Pd(II) complexes were found to act as effectual catalysts in coupling reactions. Many heterogenized systems have been based by supporting the salen Pd(II) complexes on some supports, such as silica, and magnetite nanoparticles for reuse of the catalysts. However, most of the catalytic systems suffer from rough reaction conditions and disappointing catalytic efficiency.[1–10]

Morphology-controlled nanomaterials such as silica play a decisive role in the development of technologies for addressing challenges in the fields of wellness, environment, and energy. Mesoporous silica materials discovery such as MCM-41 and SBA-15, a notable increase in the design. It was synthesis of nanosilica with different sizes, shapes, morphologies, and tissue properties has been observed in lately years. KCC-1 is dendritic fibrous nanosilica as one notable invention that have a unique fibrous morphology, unlike the tubular porous structure of various customary silica materials. It has a high surface area with improved accessibility to the internal surface, tunable pore size and pore volume, controllable particle size, and, importantly, improved stability.[11–20]

In recent years, magnetic nanoparticles of iron oxide (Fe$_3$O$_4$) have been widely used as a heterogeneous catalyst in organic reactions because they are cheap, available, low toxicity,

recyclable and easy to separate from the reaction solution using a magnet.[21,22] Lately, organometallic ionic complexes (OICs) have emerged as very marvelous catalysts because they can be created from readily available and highly tailorable metal and ligand forerunners for multifunctional integration.[23,24] Many researchers have showned OICs that contain a Lewis acidic metal center and a nucleophilic halogen anion (X$^-$) portion as highly impressive bifunctional catalysts for the coupling reaction between carbon dioxide and other organic compound under co-catalyst free circumstances owing to the cooperative effects of the catalytic functional groups.[25–27] Having this point in mind, we envisioned a way in which the preface of Lewis acid (metal center) active sites to a halogen anion (X$^-$) based ionic polymer could provide highly active, recyclable catalysts for the synthesis of heterocyclic compounds. In continued our research, we've replaced the organic groups with silica groups. Our study illustrated that the APTPOSS was a powerful and highly efficient support for the strength of the catalyst structure. Our goal was to enhance the strength of the catalyst structure by this replacement. This catalyst support *via* obstruction of Fe$_3$O$_4$/KCC-1 by APTPOSS (Fe$_3$O$_4$/KCC-1/APTPOSS). In fact, Fe$_3$O$_4$/KCC-1/APTPOSS is a nano labyrinth to hold the structure. We believe that this unique property will be very useful for the design of silica-supported catalysts, for which the accessibility of active sites can be increased significantly. Herein, we report the design and synthesis of a novel bifunctional complex composed of the cross-linked Fe$_3$O$_4$/KCC-1/APTPOSS as a substrate with the *N*,*N*′-bis({4-dimethylamino}salicylidene) ethylenediamino palladium(II) (salen-Pd(II)) Schiff base outer shell to serve as a catalyst for the synthesis pentafulvene (Scheme 1). It is noteworthy that this is the first report on the synthesis of magnetic nanoparticles that can be reused up to ten times without significant loss of catalytic activity.

*aDepartment of New Materials, Institute of Science and High Technology and Environmental Sciences, Graduate University of Advanced Technology, PO Box 76315-117, Kerman, Iran. E-mail: ahassankhani@gmail.com*

*bYoung Researchers and Elite Club, Neyshabur Branch, Islamic Azad University, Neyshabur, Iran*

# Experimental

## Materials and methods

Chemical materials were purchased from Fluka and Merck in high purity. Melting points were determined in open capillaries using an Electrothermal 9100 apparatus and are uncorrected. FTIR spectra were recorded on a VERTEX 70 spectrometer (Bruker) in the transmission mode in spectroscopic grade KBr pellets for all the powders. The particle size and structure of nano particle was observed by using a Philips CM10 transmission electron microscope operating at 100 kV. Powder X-ray diffraction data were obtained using Bruker D8 Advance model with Cu kα radiation. The thermogravimetric analysis (TGA) was carried out on a NETZSCH STA449F3 at a heating rate of 10 °C min$^{-1}$ under nitrogen. $^1$H and $^{13}$C NMR spectra were recorded on a BRUKER DRX-300 AVANCE spectrometer at 300.13 and 75.46 MHz, BRUKER DRX-400 AVANCE spectrometer at 400.22 and 100.63 MHz, respectively. Elemental analyses for C, H, and N were performed using a Heraeus CHN–O-Rapid analyzer. The purity determination of the products and reaction monitoring were accomplished by TLC on silica gel polygram SILG/UV 254 plates. Mass spectra were recorded on Shimadzu GCMS-QP5050 Mass Spectrometer.

## General procedure for the preparation of Fe$_3$O$_4$ MNPs

The synthesis procedure is illustrated as follows: (1) 0.01 mol FeCl$_2$·4H$_2$O and 0.03 mol FeCl$_3$·6H$_2$O were dissolved in to 200 mL distilled water, followed by the addition of polyethylene glycol (PEG) (1.0 g, MW 6000). (2) Sodium hydroxide (NaOH) was added to the solution and the pH value was controlled in the range 12 ≤ pH ≤ 13. (3) 5 mL of hydrazine hydrate (N$_2$H$_4$·H$_2$O, 80% concentration) was added to the above suspension. The reaction was continued for about 24 h at room temperature. During this period, the pH value was adjusted by NaOH and kept in the range 12 ≤ pH ≤ 13. The black Fe$_3$O$_4$ NPs were then rinsed several times with ionized water.

## General procedure for the preparation of Fe$_3$O$_4$/SiO$_2$ MNPs

0.02 mol of Fe$_3$O$_4$ MNPs were dispersed in a mixture of 80 mL of ethanol, 20 mL of deionized water and 2.0 mL of 28 wt% concentrated ammonia aqueous solution (NH$_3$·H$_2$O), followed by the addition of 0.20 g of tetraethyl orthosilicate (TEOS). After vigorous stirring for 24 h, the final suspension was repeatedly washed, filtered for several times and dried at 60 °C in the air.

## General procedure for the preparation of Fe$_3$O$_4$/SiO$_2$/KCC-1 MNPs

Fe$_3$O$_4$/SiO$_2$ (0.25 g) was dispersed in an aqueous solution (30 mL) containing urea (0.3 g) to form solution A under ultra-sonication for 1 h. Cetylpyridinium bromide (CPB) (0.5 g) was added to 0.75 mL of n-pentanol and 30 mL cyclohexane to from solution B. Solution A was added to solution B under stirring at room temperature. Then 1.25 g TEOS was added drop wise to the abovementioned solution. The resulting mixture was continually stirred for 1 h at room temperature and then placed into a 120 °C environment for 5 h, thus inciting the reaction. After the reaction was completed, the mixture was allowed to cool to room temperature, and the Fe$_3$O$_4$/SiO$_2$/KCC-1 core–shell microspheres were isolated by strong magnetic suction, then washed with deionized water and acetone, and dried overnight in a drying oven at 40 °C. This material was then calcined at 550 °C for 5 h in air.

**Preparation of octakis[3-(3-aminopropyltriethoxysilane)propyl] octasilsesquioxane (APTPOSS).** 3-Aminopropyltriethoxysilane (20 mmol) and ClPOSS (2 mmol) were transferred to a reaction vessel under nitrogen atmosphere and the reaction solution was stirred at 100 °C for 2 days. Then the mixture was cooled to room temperature and the solution was filtered and washed with methanol and acetone.[28]

## General procedure for the preparation of Fe$_3$O$_4$/KCC-1/APTPOSS MNPs

Fe$_3$O$_4$/KCC-1 MNPs (2 mmol) and THF (20 mL) were mixed together in a beaker, and then NaH (20 mmol) was dispersed in to the mixture by ultrasonication. APTPOSS (0.5 g) was added at room temperature and stirred for another 16 h at 60 °C. The
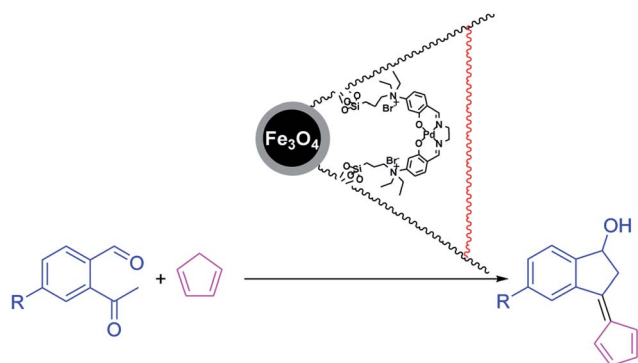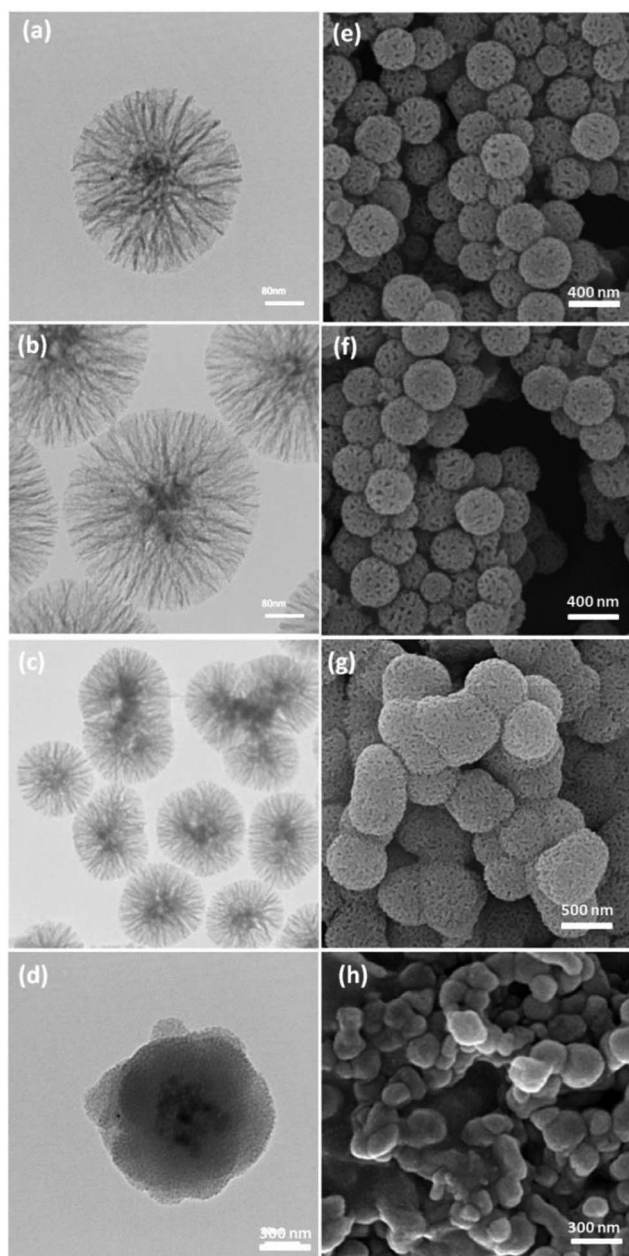


Scheme 1  Synthesis of pentafulvene in the presence of Fe$_3$O$_4$/KCC-1/APTPOSS/salen/Pd(ii) MNPs.
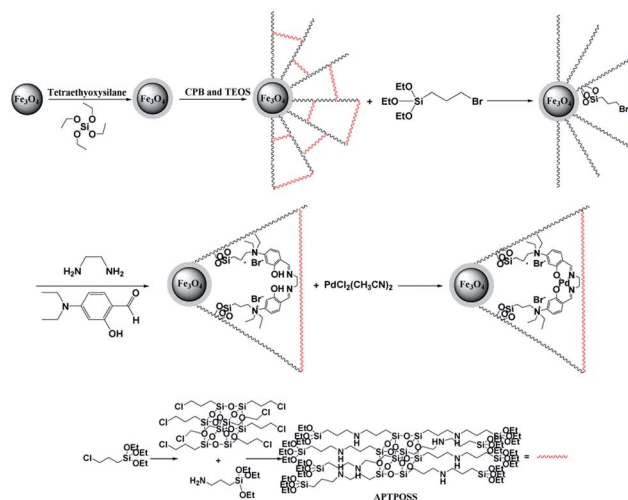


Scheme 2  Schematic illustration of the synthesis for Fe$_3$O$_4$/KCC-1/APTPOSS/salen/Pd(ii) MNPs.

**Fig. 1** TEM images of Fe₃O₄/KCC-1 MNPs (a); fresh Fe₃O₄/KCC-1/APTPOSS/salen/Pd(II) MNPs (b); Fe₃O₄/KCC-1/APTPOSS/salen/Pd(II) MNPs after ten reuses (c); Fe₃O₄/KCC-1/salen/Pd(II) MNPs after ten reuses (d); FE-SEM images of Fe₃O₄/KCC-1 MNPs (e); fresh Fe₃O₄/KCC-1/APTPOSS/salen/Pd(II) MNPs (f); Fe₃O₄/KCC-1/APTPOSS/salen/Pd(II) MNPs after ten reuses (g); Fe₃O₄/KCC-1/salen/Pd(II) MNPs after ten reuses (h).

resultant products were collected and washed with ethanol and deionized water in sequence, and then dried under vacuum at 60 °C for 2 h for further use.

**General procedure for the preparation of salen**

Diethylamine (0.30 g) was added to a solution of 4-(diethylamino)salicylaldehyde (2.00 g) in ethanol (30 mL). The reaction mixture was heated at reflux for 24 h then the mixture was

cooled to room temperature. After 48 h, the precipitated yellow crystals were separated by filtration, washed with ethanol, and dried at 80 °C for 12 h to give the salen ligand.

**General procedure for the preparation of Fe₃O₄/KCC-1/APTPOSS/3-bromopropyl MNPs**

Under nitrogen atmosphere, 2 mL of 3-bromopropyltrimethoxysilane is added to 5.0 g of Fe₃O₄/KCC-1/APTPOSS in suspension with 50 mL of freshly distilled toluene. After 24 h of reaction under reflux, the resulting solid was separated using a magnet, washed thoroughly with toluene, ethanol, and then subjected to toluene Soxhlet extraction. The functionalized Fe₃O₄/KCC-1 is finally dried in vacuum at 70 °C.

**General procedure for the preparation of Fe₃O₄/KCC-1/APTPOSS/salen MNPs**

The salen ligand (0.41 g) was dissolved in toluene (5 mL) and methanol (5 mL), respectively. The two solutions were combined and the reaction mixture was vigorously stirred at 60 °C for 24 h then Fe₃O₄/KCC-1/APTPOSS/3-bromopropyl (0.6 g) was added. After stirring at 60 °C for 24 h, the brown solid was separated by external magnet, washed with ethanol, and dried under vacuum at 60 °C for 24 h to afford Fe₃O₄/KCC-1/APTPOSS/salen.

**General procedure for the preparation of Fe₃O₄/KCC-1/APTPOSS/salen/Pd(II) MNPs**

A mixture of Fe₃O₄/KCC-1/APTPOSS/salen (0.45 g), PdCl₂(CH₃CN)₂ (0.5 g), and Et₃N (0.8 mL) in methanol (10 mL) was degassed with N₂ and refluxed for 4 h. After cooling to room temperature, the precipitate was filtered and washed with methanol (10 mL × 3) and ether (10 mL × 3) to get a powder. The final particle was separated from the solution by external magnet, washed three times with water to remove any ions present, and dried under vacuum.

**General procedure for the synthesis of pentafulvene**

A mixture of 2-acetyl-benzaldehyde (10 mmol), cyclopentadiene (70 mmol), and nano Fe₃O₄/KCC-1/APTPOSS/salen/Pd(II) MNPs (6 mg) and DMF (20 mL) were stirred at room temperature for the 3 h. Upon completion, the progress of the reaction was monitored by TLC when the reaction was completed, the nano KCC-1/salen/Pd(II) NPs were separated by external magnet. The solvent was removed under reduced pressure, and the residue was purified by flash column chromatography over silica gel (EtOAc/hexanes, 1 : 5) to yield the desired pentafulvene.

## Results and discussion

The salen–Pd Schiff base was covalently attached onto the surface of Fe₃O₄/KCC-1/APTPOSS by a nucleophilic reaction, which resulted in dual catalytically active centers with a synergistic effect to greatly enhance the catalytic productivity. Furthermore, the catalyst can be easily recovered from the reaction mixture by centrifugation for steady reuse (Scheme 2).
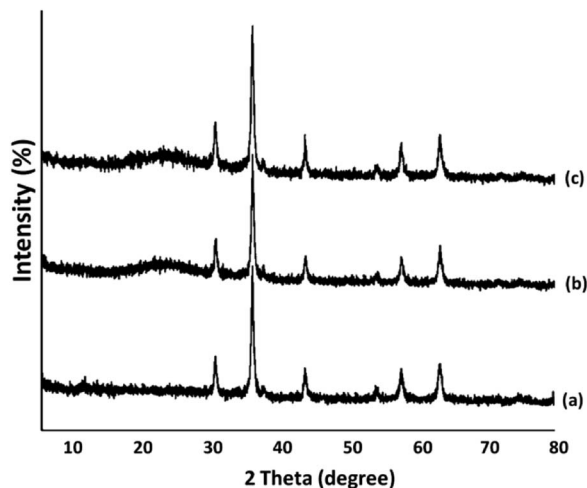
**Fig. 2** XRD analysis of (a) $Fe_3O_4$, (b) $Fe_3O_4/KCC-1$, and (c) $Fe_3O_4/KCC-1/APTPOSS/salen/Pd(\text{II})$ MNPs.
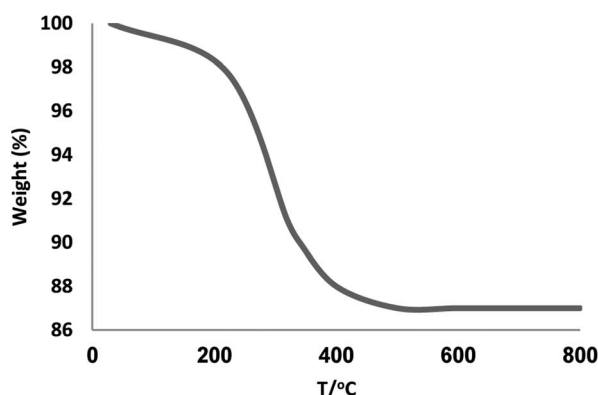


**Fig. 3** TGA diagram of $Fe_3O_4/KCC-1/APTPOSS/salen/Pd(\text{II})$ MNPs.



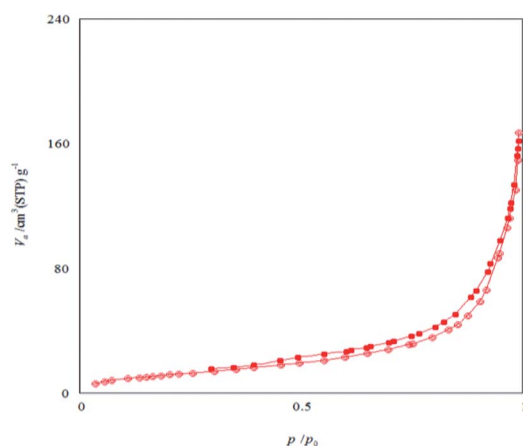**Fig. 4** Adsorption–desorption isotherms of $Fe_3O_4/KCC-1/APTPOSS/salen/Pd(\text{II})$ MNPs.

The morphology and structure of the $Fe_3O_4/KCC-1/APTPOSS$ and $Fe_3O_4/KCC-1/APTPOSS/salen/Pd(\text{II})$ MNPs are further characterized by TEM and FE-SEM. As shown in Fig. 1a, the $Fe_3O_4/$

KCC-1/APTPOSS possesses a core of $Fe_3O_4$ particle, nonporous silica layer and silica fibres. The as-prepared magnetic core–shell fibrous silica material $Fe_3O_4/KCC-1$ with fibrous structure was uniform and monodispersed. Also, TEM and FE-SEM images of highly textured $Fe_3O_4/KCC-1$ samples, where the samples have spheres of uniform size with diameters of ~300 nm and a wrinkled radial structure (Fig. 1a and e). A close inspection of these images shows that wrinkled fibers (with thicknesses of ~8.5 nm) grow out from the center of the spheres and are arranged radially in three dimensions. Also, the overlapping of the wrinkled radial structure forms cone-shaped open pores. The TEM and FE-SEM images shows that the entire sphere is solid and composed of fibers. Furthermore, this open hierarchical channel structure and fibers are more easily for the mass transfer of reactants and increase the accessibility of active sites. The FE-SEM and TEM images of $Fe_3O_4/KCC-1/salen/Pd(\text{II})$ MNPs showed that after modification the morphology of $Fe_3O_4/KCC-1$ is not change (Fig. 1b and f). To assess the exact impact of the presence of APTPOSS in the catalyst, the $Fe_3O_4/KCC-1/APTPOSS/salen/Pd(\text{II})$ compared with $Fe_3O_4/KCC-1/salen/Pd(\text{II})$ MNPs. To further understand this issue, compared FE-SEM and TEM images of used catalyst with those of the fresh catalyst. Comparison of FE-SEM and TEM images of used catalyst with those of the fresh catalyst showed that the morphology and structure of $Fe_3O_4/KCC-1/APTPOSS/salen/Pd(\text{II})$ and $Fe_3O_4/KCC-1/salen/Pd(\text{II})$ MNPs remained intact after ten recoveries. Fig. 1d and h shows degradation of structure of $Fe_3O_4/KCC-1/salen/Pd(\text{II})$ MNPs in the reuse process. Its fiber structure has been destroyed. But, the functionalization of the $Fe_3O_4/KCC-1/APTPOSS/salen/Pd(\text{II})$ MNPs does not result in the change of the morphology (Fig. 1c and g). These study proves, this stable on structure of $Fe_3O_4/KCC-1/APTPOSS/salen/Pd(\text{II})$ MNPs were due to the presence of APTPOSS in the catalyst structure. APTPOSS can be a strong scaffold in KCC-1 structure.

The powder X-ray diffraction patterns of $Fe_3O_4$, $Fe_3O_4/KCC-1$, and $Fe_3O_4/KCC-1/APTPOSS/salen/Pd(\text{II})$ MNPs are shown in Fig. 2. As can be observed, all samples possess the typical diffraction peaks at (220), (311), (400), (422), (511) and (440), which are in good agreement with the data for standard $Fe_3O_4$ sample, as reported in the JCPDS card (no. 19-0629) (Fig. 2a). Besides the peak of iron oxide, the XRD pattern of $Fe_3O_4/KCC-1/APTPOSS$ core–shell nanoparticles presented a broad featureless XRD peak at low diffraction angle, which corresponded to the amorphous silica (Fig. 2b). Fig. 2c shows a typical XRD pattern of the $Fe_3O_4/KCC-1/APTPOSS/salen/Pd(\text{II})$ MNPs. There was no change in it.

To confirm the thermal stability of the $Fe_3O_4/KCC-1/APTPOSS/salen/Pd(\text{II})$ MNPs, the thermogravimetric analysis of this material was performed at temperatures ranging from room temperature to 700 °C (Fig. 3). The weight loss below 250 °C was ascribed to the elimination of the physisorbed and chemisorbed solvent on the surface of the silica material. About 11.6% of the weight loss, in the temperature range 250–450 °C, was due to the organic group derivatives.

The $N_2$ adsorption–desorption isotherms of $Fe_3O_4/KCC-1/APTPOSS/salen/Pd(\text{II})$ MNPs showed characteristic type IV
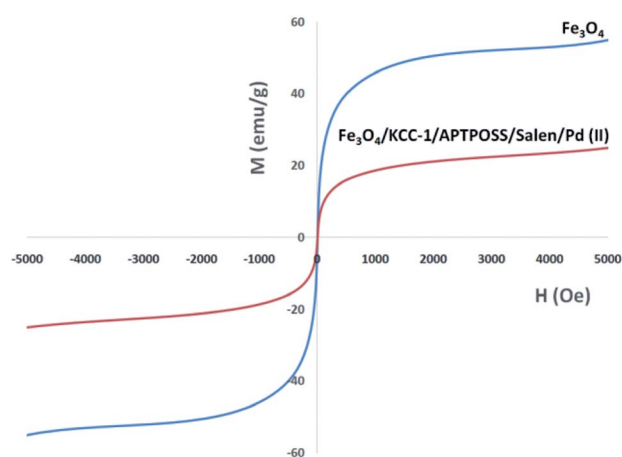
**Table 1** Structural parameters of Fe$_3$O$_4$/KCC-1 and Fe$_3$O$_4$/KCC-1/APTPOSS/salen/Pd(II) MNPs materials determined from nitrogen sorption experiments

| Catalysts | $S_{BET}$ (m$^2$ g$^{-1}$) | $V_a$ (cm$^3$ g$^{-1}$) | $D_{BJH}$ (nm) |
|---|---|---|---|
| Fe$_3$O$_4$/KCC-1 | 427 | 1.23 | 14.51 |
| Fe$_3$O$_4$/KCC-1/APTPOSS/salen/Pd(II) | 311 | 0.98 | 11.16 |

curve (Fig. 4), which is consistent with literature reports on standard fibrous silica spheres. As for Fe$_3$O$_4$/KCC-1, the BET surface area, total pore volume, and BJH pore diameter are obtained as 427 m$^2$ g$^{-1}$, 1.23 cm$^3$ g$^{-1}$, and 14.51 nm respectively, whereas the corresponding parameters of Fe$_3$O$_4$/KCC-1/APTPOSS/salen/Pd(II) MNPs have decreased to 311 m$^2$ g$^{-1}$, 0.98 cm$^3$ g$^{-1}$, and 11.16 nm. The nitrogen sorption analysis of Fe$_3$O$_4$/KCC-1/salen/Pd(II) MNPs also confirms a regular and uniform mesostructure with a decrease in surface area, pore diameter and pore volume parameters in comparison with that of pristine Fe$_3$O$_4$/KCC-1. With the functionalization by salen/Pd–Si, the corresponding pore volumes are drastically reduced. This could be ascribed to increased loading with the sensing probe, which occupies a large volume inside the silica spheres (Fig. 4 and Table 1).

The magnetic properties of the nanoparticles were characterized using a vibrating sample magnetometer (VSM). The magnetization curves of the obtained nanocomposite registered at 300 K show nearly no residual magnetism is detected (Fig. 5), which means that the nanocomposite exhibited the paramagnetic characteristics. Magnetic measurement shows that pure Fe$_3$O$_4$, and Fe$_3$O$_4$/KCC-1/APTPOSS/salen/Pd(II) have saturation magnetization values of 55.1, and 22.4 emu g$^{-1}$ respectively. These nanocomposites with paramagnetic characteristics and high magnetization values can quickly respond to the external magnetic field and quickly redisperse once the external magnetic field is removed. The result reveals that the nanocomposite exhibit good magnetic responsible, which suggests a potential application for targeting and separation.



**Fig. 6** Magnetic separation ability of Fe$_3$O$_4$/KCC-1/APTPOSS/Pd(II) MNPs.

In addition, as seen in Fig. 6, by putting a magnet nearby the reaction mixture balloons can be seen the magnetic separation ability of catalyst. The magnet will attract the magnetic nanoparticles towards itself, and when the external magnet is removed, the catalyst will scatter in the solution with little shake.

FT-IR spectroscopy was employed to determine the surface modification of the synthesized catalyst (Fig. 7). The Si–O–Si symmetric and asymmetric stretching vibrations at 793 cm$^{-1}$ and 1091 cm$^{-1}$ and the O–H stretching vibration at 3430 cm$^{-1}$ were observed for the Fe$_3$O$_4$/KCC-1 (Fig. 7a). The bands observed at 3121 and 2929 cm$^{-1}$ are assigned to C–H stretching of aromatic and aliphatic moieties. Moreover, the signals cleared at 1462 and 1632 cm$^{-1}$ are, respectively, attributed to C=C and C=N. (Fig. 7b). These results indicated that the salen had been successfully introduced onto the surface of Fe$_3$O$_4$/KCC-1.

To optimize reaction conditions for the Fe$_3$O$_4$/KCC-1/APTPOSS/salen/Pd(II) MNPs catalyst system, the effects of various reaction parameters were investigated. We examined the effect of solvent on the synthesis of pentafulvene using the Fe$_3$O$_4$/



**Fig. 5** Room-temperature magnetization curves of the nano catalysis.
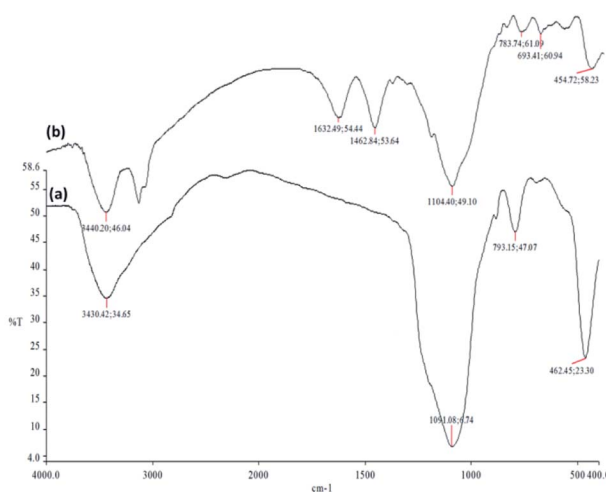


**Fig. 7** FTIR spectra of (a) Fe$_3$O$_4$/KCC-1 MNPs, (b) Fe$_3$O$_4$/KCC-1/APTPOSS/salen/Pd(II) MNPs.

**Table 2** The effect of solvent and temperature for synthesis of pentafulvene[a]

| Entry | Solvent | Temp. (°C) | Yield[b] (%) |
|---|---|---|---|
| 1 | DMF | Reflux | 80 |
| 2 | DMF | 130 | 85 |
| 3 | DMF | 110 | 92 |
| 4 | DMF | 90 | 92 |
| 5 | DMF | 70 | 92 |
| 6 | DMF | 50 | 92 |
| 7 | DMF | r.t. | 92 |
| 8 | DMSO | r.t. | 74 |
| 9 | Dioxane | r.t. | 82 |
| 10 | $CH_3CN$ | r.t. | 69 |
| 11 | $CH_2Cl_2$ | r.t. | 77 |
| 12 | EtOAc | r.t. | 82 |
| 13 | THF | r.t. | 74 |
| 14 | Toluene | r.t. | 69 |
| 15 | $CHCl_3$ | r.t. | 77 |
| 16 | n-Hexane | r.t. | 21 |
| 17 | Benzene | r.t. | 17 |
| 18 | $CCl_4$ | r.t. | 15 |
| 19 | Cyclohexane | r.t. | 10 |
| 20 | $H_2O$ | r.t. | 29 |
| 21 | EtOH | r.t. | 21 |
| 22 | i-PrOH | r.t. | 32 |
| 23 | MeOH | r.t. | 18 |
| 24 | Solvent-free | r.t. | — |

[a] Reaction conditions: 2-acetyl-benzaldehyde (10 mmol), cyclopentadiene (70 mmol), and nano $Fe_3O_4$/KCC-1/APTPOSS/salen/Pd(II) MNPs (6 mg), and solvent (10 mL), 3 h. [b] GC yields [%].

KCC-1/APTPOSS/salen/Pd(II) MNPs (Table 2). Solvent does affect on catalysts performance. n-Hexane, benzene, $CCl_4$, or cyclohexane, an non-polar solvent, gave pentafulvene a lower yield (Table 2, entry 16–19). Also, i-PrOH, MeOH, EtOH, and $H_2O$, protic polar solvents, gave also pentafulvene in low yields (Table 2, entry 20–23). The reaction was do better in aprotic polar solvent. $CH_3CN$, THF, $CH_2Cl_2$, THF, toluene, dioxane, $CHCl_3$, EtOAc, and DMSO gave pentafulvene in good yields (Table 2, entries 4–12). In this study, it was found that DMF is a more efficient (Table 2, entry 7) over other solvents. A solvent that stabilizes one of two competing transition states that control the selectivity should enhance the selectivity of the product obtained via the stabilized transition state. We also investigated
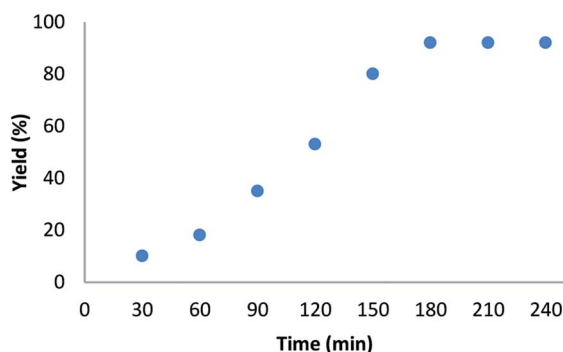
**Fig. 8** Effect of time on yield of pentafulvene.
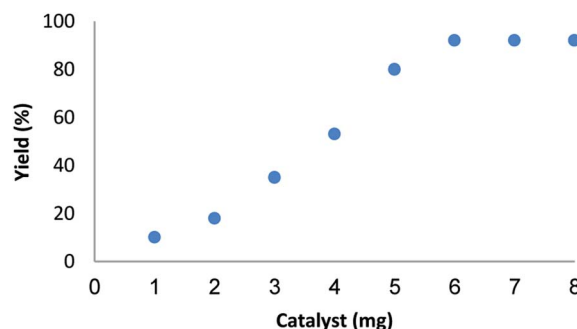
**Fig. 9** Effect of increasing amount of $Fe_3O_4$/KCC-1/APTPOSS/salen/Pd(II) NPs on yield of pentafulvene.

the crucial role of temperature in the synthesis of pentafulvene in the presence of $Fe_3O_4$/KCC-1/APTPOSS/salen/Pd(II) MNPs as a catalyst. Results clearly indicated that the catalytic activity is sensitive to reaction temperature. The yield decreased when the temperature reached 130 °C. The best temperature for this reaction was at room temperature (Table 2, entry 1–7).

The influence of time on this reaction is exhibited in Fig. 8. It is obvious that the pentafulvene yield increased up to 92% for 180 min. Whereas further increase in the time don't resulted in a slight decrease in the product yield. Therefore, the optimal time for synthesis of pentafulvene is 180 min.

The amount of catalyst is another important factor in current reaction for the synthesis of pentafulvene (Fig. 9). As shown in Fig. 9, in the absence of the catalyst no product was obtained. When 1–5 mg of catalyst was elaborated on sample reaction, moderate yields of product was obtained. The best result was achieved when the model reaction was carried out in the presence of 6 mg of catalyst. A rise in the catalyst amount showed no upgrading in the model reaction.

For further investigation the efficiency of the catalyst, different control experiments were performed and the obtained information is shown in Table 3. Initially, a standard reaction was carried out using $Fe_3O_4$/KCC-1/APTPOSS showed that any amount of the desired product was not formed after 60 min of reaction time (Table 3, entries 1). Also, when $Fe_3O_4$/KCC-1/APTPOSS/salen was used as the catalyst, a reaction was not observed (Table 3, entries 2). The salen could not give the satisfactory catalytic activity under mild reactions. Based on
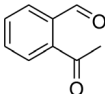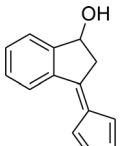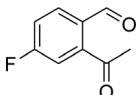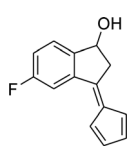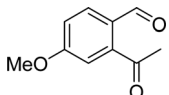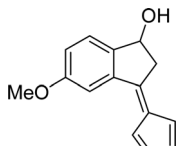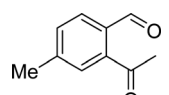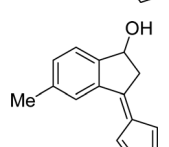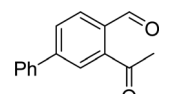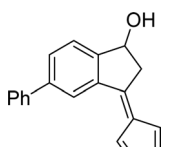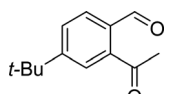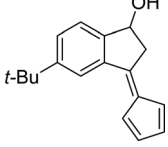
**Table 3** Influence of different catalysts for synthesis of pentafulvene[a]

| Entry | Catalyst | Yield[b] (%) |
|---|---|---|
| 1 | KCC-1 | — |
| 2 | $Fe_3O_4$/KCC-1/APTPOSS | — |
| 3 | $Fe_3O_4$/KCC-1/APTPOSS/salen/Pd(II) | 92 |
| 4 | Nano-$SiO_2$/salen/Pd(II) | 53 |
| 5 | MCM-41/salen/Pd(II) | 74 |
| 6 | SBA-15/salen/Pd(II) | 80 |
| 7 | Salen/Pd(II) | 83 |

[a] Reaction conditions: 2-acetyl-benzaldehyde (10 mmol), cyclopentadiene (70 mmol), and catalyst (6 mg), at room temperature for 3 h. [b] Isolated yield.

**Table 4** Reaction of various 2-acetyl-benzaldehydes with cyclopentadiene in the presence of Fe$_3$O$_4$/KCC-1/APTPOSS/salen/Pd(II) MNPs[a]

| Entry | 2-Acetyl-benzaldehyde | Product | Yield[b] (%) |
|---|---|---|---|
| 1 | | | 92 |
| 2 | F | F | 94 |
| 3 | MeO | MeO | 89 |
| 4 | Me | Me | 87 |
| 5 | Ph | Ph | 90 |
| 6 | t-Bu | t-Bu | 91 |

[a] Reaction conditions: 2-acetyl-benzaldehyde (10 mmol), cyclopentadiene (70 mmol), and catalyst (6 mg), at room temperature for 3 h. [b] Isolated yields (%).
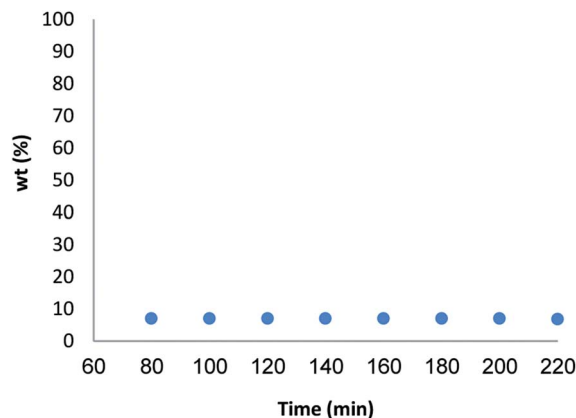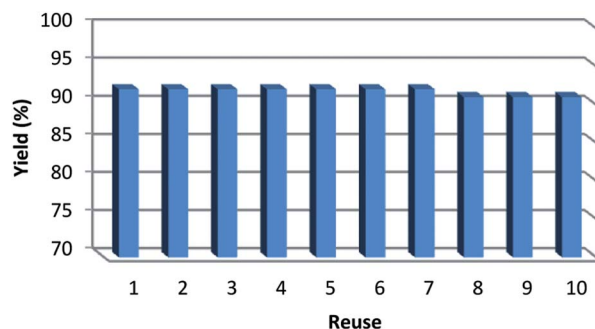


**Fig. 10** Time-dependent correlation of the palladium leaching in model reaction.

investigations because of its high reactivity, high selectivity and easy separation. Also, the activity and selectivity of nano-catalyst can be manipulated by tailoring chemical and physical properties like size, shape, composition and morphology. To assess the exact impact of the presence of KCC-1 in the catalyst, the Fe$_3$O$_4$/KCC-1/APTPOSS/salen/Pd(II) MNPs compared with MCM-41/salen/Pd(II), SBA-15/salen/Pd(II), and nano-SiO$_2$/salen/Pd(II). When nano-SiO$_2$/salen/Pd(II), MCM-41/salen/Pd(II) or SBA-15/salen/Pd(II) was used as the catalyst, the yield of the desired product was average to good, but the yield for Fe$_3$O$_4$/KCC-1/APTPOSS/salen/Pd(II) MNPs was excellent. Non-negligible activity of the silica was attributed to its shape, composition and morphology. Besides, the large space between fibers can significantly increase the accessibility of the active sites of the KCC-1. That is why, the KCC-1 was more effective than nano-SiO$_2$, MCM-41, and SBA-15 (Table 3, entries 3–6). As a result, KCC-1 NPs were used in the subsequent investigations because of its high reactivity, high selectivity and easy separation (Table 3).

To examine the scope of the catalytic properties of the catalyst for synthesis of pentafulvene, various types of 2-acetyl-benzaldehydes was reacted with cyclopentadiene in the presence of a catalytic amount of Fe$_3$O$_4$/KCC-1/APTPOSS/salen/Pd(II) MNPs. Furthermore, electron rich and electron poor 2-acetyl-benzaldehydes react smoothly with cyclopentadiene in similar reaction conditions. The electron rich allylarene show good

these disappointing results, we continued the studies to improve the yield of the product by added the Pd(II). Notably, there was difference in the reaction yields when reaction was carried out using Fe$_3$O$_4$/KCC-1/APTPOSS/salen/Pd(II) NPs and salen/Pd(II) catalyst (Table 3, entries 3 and 7). These results showed catalytic properties of N$^+$Cl$^-$ in this structure. These results indicate that both of Pd(II) and ionic structure (N$^+$Cl$^-$) in this catalyst will maximize the catalyst performance. Also, salen/Pd(II) is not recoverable and reusable for the next runs. These observations show that the reaction cycle is mainly catalyzed by Pd(II) species complexed on the Fe$_3$O$_4$/KCC-1/APTPOSS/salen nanostructure. The nano-sized particles increase the exposed surface area of the active site of the catalyst, thereby enhancing the contact between reactants and catalyst dramatically and mimicking the homogeneous catalysts. As a result, Fe$_3$O$_4$/KCC-1/APTPOSS/salen/Pd(II) MNPs was used in the subsequent



**Fig. 11** The reusability of catalysts for synthesis of pentafulvene.
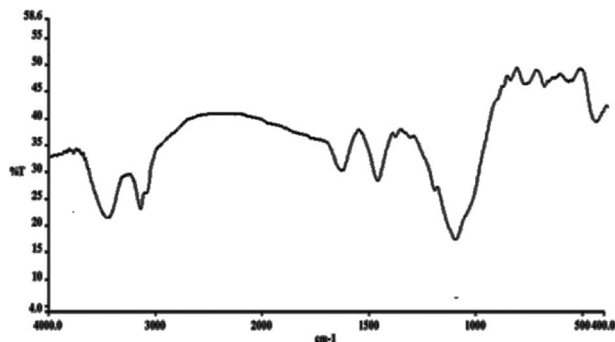
Fig. 12 FTIR spectra of $Fe_3O_4$/KCC-1/APTPOSS/salen/Pd(II) MNPs after ten reuses.

reactivity (90–94% yield) for the formation of the corresponding products in the C–C and C–H coupling reaction under similar reaction conditions. The relative reactivity of 2-acetyl-benzaldehydes towards the Pd(II) centre decreases in the order: MeO > Me (Table 4, entry 3 and 4). As shown in Table 4, C–C and C–H coupling reaction of cyclopentadiene with fluoro-2-acetyl-benzaldehyde proceeds smoothly under mild reaction conditions giving the reaction condition in excellent yields (Table 4, entries 2).

For further investigation the possibility of the heterogeneous nature of $Fe_3O_4$/KCC-1/APTPOSS/salen/Pd(II) MNPs, a kinetic study was performed. For this purpose, copper leaching was study for synthesis of pentafulvene under the optimized reaction condition. To determine the Pd(II) concentration in solution, five samples of the reaction mixture were taken during the reaction. The samples were analyzed by ICP-MS as well as the yield of the reaction was monitored by GC. The results were described in Fig. 10. No obvious leaching was observed, according to the ICP-MS data. According to the obtained results, the conclusion could be derived that the heterogenous palladium species aren't the catalyst promoter in this reaction.

It is important to note that the heterogeneous property of $Fe_3O_4$/KCC-1/APTPOSS/salen/Pd(II) MNPs facilitates its efficient recovery from the reaction mixture during work-up procedure. The activity of the recycled catalyst was also examined under the optimized conditions. After the
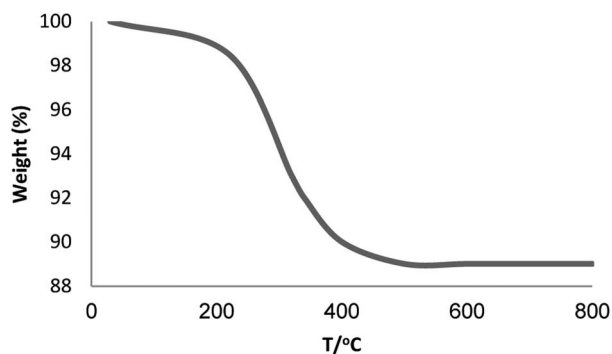
**Table 5** The loading amount of Pd(II) in $Fe_3O_4$/KCC-1/APTPOSS/salen/Pd(II) MNPs

| Entry | Catalyst | wt% |
|-------|----------|-----|
| 1 | $Fe_3O_4$/KCC-1/APTPOSS/salen/Pd(II) | 1.7 |
| 2 | $Fe_3O_4$/KCC-1/APTPOSS/salen/Pd(II) after ten reuses | 1.6 |

completion of reaction, the catalyst was separated by filtration, washed with methanol and dried at the pump. The recovered catalyst was reused for ten consecutive cycles without any significant loss in catalytic activity (Fig. 11). This lack of reduction in catalyst performance can be attributed to the simple and stability of the catalyst structure. Comparison of FT-IR spectra of used catalyst with those of the fresh catalyst showed that the structure of salen remained intact after ten recoveries (Fig. 12). Also, the loading amount of salen in the fresh $Fe_3O_4$/KCC-1/APTPOSS/salen/Pd(II) and $Fe_3O_4$/KCC-1/APTPOSS/salen/Pd(II) after ten reuses as determined by TGA. The amount of salen in $Fe_3O_4$/KCC-1/APTPOSS/salen/Pd(II) after ten reuses was almost equal to the fresh $Fe_3O_4$/KCC-1/APTPOSS/salen/Pd(II) (Fig. 13). Also, the contents of Pd(II) in catalyst before and after reaction were 1.7% and 1.6% respectively, determined by ICP-MS. These indicate that most of Pd(II) species leaching into solution are recaptured onto the fibers of KCC-1 after completion of the reaction (Table 5).

## Conclusions

In the present study $Fe_3O_4$/KCC-1/APTPOSS/salen/Pd(II) MNPs was synthesized and characterized as an environmentally-friendly nanocatalyst for the synthesis of pentafulvenes with various electronically diverse substrates. The experimental results displayed the core–shell structure of the synthesized catalyst with a mean size range of 250–300 nm. In addition, the catalyst was easily recoverable and reusable. Subsequently, high yields in short reaction times were achieved without the need for an expensive catalyst as well as excellent reusability for at least ten times in the corresponding reaction without a reduction in catalytic activity.

## Conflicts of interest

There are no conflicts to declare.

## Acknowledgements

## Notes and references

1 P. Liu, X.-J. Feng and R. He, *Tetrahedron*, 2010, **66**, 631–636.
2 S. Nasifa, B. Biplab and D. Pankaj, *Tetrahedron Lett.*, 2013, **54**, 2886–2889.



Fig. 13 TGA image of $Fe_3O_4$/KCC-1/APTPOSS/salen/Pd(II) MNPs after ten reuses.

3  N. T. S. Phan and P. Styring, *Green Chem.*, 2008, **10**, 1055–1060.

4  T. Kylmala, N. Kuuloja, Y. Xu, K. Rissanen and R. Franzen, *Eur. J. Org. Chem.*, 2008, **23**, 4019–4024.

5  M. Joao Matos, S. Vazquez-Rodriguez, F. Borges, L. Santana and E. Uriarte, *Tetrahedron Lett.*, 2011, **52**, 1225–1227.

6  S. R. Borhade and S. B. Waghmode, *Tetrahedron Lett.*, 2008, **49**, 3423–3429.

7  S. R. Borhade and S. B. Waghmode, *Indian J. Chem., Sect. B: Org. Chem. Incl. Med. Chem.*, 2010, **49**, 565.

8  N. T. S. Phan, J. Khan and P. Styring, *Tetrahedron*, 2005, **61**, 12065–12073.

9  N. T. S. Phan, D. H. Brown and P. Styring, *Tetrahedron Lett.*, 2004, **45**, 7915–7919.

10  X. Jin, K. Zhang, J. Sun, J. Wang, Z. Dong and R. Li, *Catal. Commun.*, 2012, **26**, 199–203.

11  V. Polshettiwar, D. Cha, X. Zhang and J. M. Basset, *Angew. Chem.*, 2010, **49**, 9652–9656.

12  A. Maity and V. Polshettiwar, *ChemSusChem*, 2017, **10**, 3866–3913.

13  P. K. Kundu, M. Dhiman, A. Modak, A. Chowdhury and V. Polshettiwar, *ChemPlusChem*, 2016, **81**, 1142–1146.

14  P. Gautam, M. Dhiman, V. Polshettiwar and B. M. Bhanage, *Green Chem.*, 2016, **18**, 5890–5899.

15  A. Fihri, D. Cha, M. Bouhrara, N. Almana and V. Polshettiwar, *ChemSusChem*, 2012, **5**, 85–89.

16  S. M. Sadeghzadeh, *J. Mol. Catal. A: Chem.*, 2016, **423**, 216–223.

17  S. M. Sdeghzadeh, *Catal. Sci. Technol.*, 2016, **6**, 1435–1441.

18  S. M. Sadeghzadeh, *Catal. Commun.*, 2015, **72**, 91–96.

19  S. M. Sadeghzadeh, *Green Chem.*, 2015, **17**, 3059–3066.

20  Z. Dong, X. Le, X. Li, W. Zhang, C. Dong and J. Ma, *Appl. Catal., B*, 2014, **158–159**, 129–135.

21  S. M. Sadeghzadeh and M. Malekzadeh, *J. Mol. Liq.*, 2015, **202**, 46–51.

22  S. M. Sadeghzadeh, *RSC Adv.*, 2015, **5**, 17319–17324.

23  S. Bhunia, R. A. Molla, V. Kumari, S. M. Islam and A. Bhaumik, *Chem. Commun.*, 2015, **51**, 15732–15735.

24  E. K. Noh, S. J. Na, Sujith S., S. W. Kim and B. Y. Lee, *J. Am. Chem. Soc.*, 2007, **129**, 8082–8083, DOI: 10.1021/ja071290n.

25  Q. An, Z. Li, R. Graff, J. Guo, H. Gao and C. Wang, *ACS Appl. Mater. Interfaces*, 2015, **7**, 4969–4978.

26  D. Tian, B. Liu, Q. Gan, H. Li and D. J. Darensbourg, *ACS Catal.*, 2012, **2**, 2029–2035.

27  D. J. Darensbourg, W. C. Chung and S. J. Wilson, *ACS Catal.*, 2013, **3**, 3050–3057.

28  J. Safaei-Ghomi, S. H. Nazemzadeh and H. Shahbazi-Alavi, *Appl. Organomet. Chem.*, 2016, **30**, 911–916.